Physical Modelling in Geotechnics

Physical modelling of underground excavations in a random fractured rock mass

A.A. Emilio, D. Olivier, C. Marianne & G. Laura
Université de Lorraine, CNRS, GeoRessources, Ecole des Mines de Nancy, 54042 Nancy Cedex, France

A.H. Marwan
Ineris, The French National Institute for Industrial Environment and Risks, 54042 Nancy Cedex, France

ABSTRACT: The purpose of this study is to investigate the feasibility of performing a small-scale 1-g physical model of underground excavation in a stochastic fractured rock mass with fully controlled geometrical and mechanical properties. To do this, we are developing a unique tri-axial 1-g device. The rock-like material is printed with a 3DP. The phasing of this modeling includes the following steps: (i) mechanical characterization of 3DP material; (ii) geometrical description and mechanical characterization of the printed fractures; (iii) geometric modelling of the fully 3D physical model with a random (realistic) fractured network; (iv) integration of a monitoring system with embedded stress sensors and fiber optic; (v) construction performance of the final 3D physical; (vi) comparison with numerical modeling. This paper is dedicated to steps i) to iii). Uniaxial compression, three bending, and shear tests on 3DP specimens are presented. Results allow defining which prototype can be modelled with the investigated sand-3DP technology taking into account the scale factors.

Keywords: 1-g physical modelling, underground excavation, Sand-3D printing, fractured rock mass, optic fiber.

1 INTRODUCTION

Underground construction in fractured rock masses is often tied to complex operations and frustrating situations regarding security and safety. Many collapse accidents have been observed, resulting in dramatic situations. Most of these accidents are related to unpredicted or misunderstood behavior of the rock mass. Several research works have focused on modeling the behavior of fractured rock masses subject to different mechanical solicitations. They used different approaches: numerical modelling (Hauquin, 2016; Thanh & Hoang, 2013) in situ monitoring of stress and strain in the environment of the excavation (Tao et al., 2019; Xu et al., 2021), Ng small-scale physical model (Stone & Taylor, 1965) or under normal gravity (1-g).

To date, physical models under normal gravity have been widely investigated to simulate the stability of underground constructions in rock masses. The simulations usually simplify the problem into a 2D dimensional problem (Fuenkajorn & Phueakphum, 2010; Z. Li et al., 2005). Previous research in replicating fractured rock masses has mainly been concerned with the use of mixtures of cementitious material like gypsum, and fine aggregates such as sand (Yingjie et al., 2014). However, while these models are useful for producing continuous rock masses, they failed to model fractured rock masses. Efforts to replicate a jointed rock mass have been made by Fuenkajorn & Phueakphum, 2010; Son & Park, 2014 by building "brick" concrete block models. In these models the discontinuities is limited to two sets, most often orthogonal, and their mechanical properties (cohesion, friction angle, dilation, etc.) are not constrained nor repeatable, which restricts the representativeness of the natural fractured rock mass.

In this paper, we propose an innovative approach to model a fractured rock mass with a realistic small-scale (1-g) 3D physical model of a random jointed rock mass, subjected to different mechanical solicitations. An analogous material with weaker mechanical properties than rocks must be used to comply with scaling relationships. For this purpose, the 3D printing technology based on sand and phenolic liquid binder was adopted to simulate an equivalent rock mass-like (Nyembwe et al., 2016; Perras & Vogler, 2019) because of its high accuracy and repeatability. The questions, then are: (i) will the present model be able to replicate the behavior observed in naturally fractured rock masses subjected to mechanical solicitations? To do so, the first step will be to characterize the new material through several mechanical tests. (ii) What are the uncertainties and can they be quantified?

2 DIMITRI DEVICE

DIMITRI is an experimental device developed at the GeoRessources laboratory consisting of a large-scale tri-axial tool with an effective volume of 2.25 m^3 (L x W x H = 1.5 x 1.5 x 1m) (Fig. 1). Controlled pressure and / or displacements can be applied in all three spatial

directions through jacks, on 3 moving faces. The remaining horizontal faces are fixed and equipped with windows, where an excavation tool can be used for drilling underground excavations of a maximum section equal to 10 × 10cm^2. The ultimate stress and maximum displacement applied on the edges are 1.5MPa and 10cm respectively, thus allowing the generation of three-dimensional stress fields and extending to deep applications. Concurrently, an innovative monitoring system is being developed with: (i) fiber optics to measure strains and (ii) embedded stress sensors to measure the stress field.

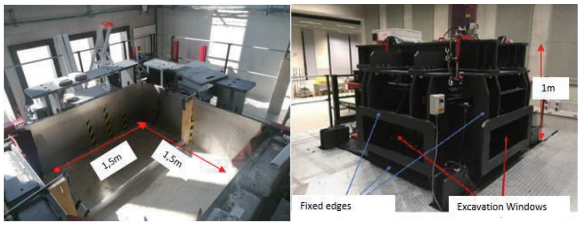

Fig. 1. Photography of Dimitri device

3 ARTIFICIAL MATERIAL: 3D- PRINTED MATERIAL

3.1 3D-printing: Binder jetting process

In this paper, the rock-like mass is constructed from artificial material based on liquid binder and sand using a Binder Jetting 3DP process. This process applies a selective binder through the inkjet head to bind sand and shape the required forms. In this study, a 3D sand printer VX1000 from Volxejet is used to manufacture specimens. The type of used sand is silica with reference GS140, and a phenolic resin as a binder. The printed layer thickness is between 250µm and 300 µm. The properties of the material depend on the level of binder saturation, the printing direction, the storage time and conditions, and the curing time and temperature (Jacques-hulin, 2019).

3.1 Artificial intact 3DP rock

A series of uniaxial compressive and three-point bending tests were performed to characterize the macro mechanical behavior (uniaxial compressive strength (UCS), Young's modulus (E), and tensile strength (σ_t)) of the 3D printed rock. Two types of specimens: cylinder (D=38mm, H=76mm), and bar (l=e=34mm, L=150mm) were printed. Since the 3D printing process involves possible mechanical anisotropy, the specimens are printed in three perpendicular X, Y, and Z directions, with three different binders saturation rates 6.5% (stander rate), 5.7% (intermediary rate), and 5% (minimum rate to assure the cohesion of the material).

During the uniaxial compressive tests, all specimens are loaded (strain) at a controlled rate of 0.2mm/s until failure, while a loading rate of 0.1mm/s or 0.05mm/s is applied during the three-point bending tests. All specimens are tested at room temperature and after the same storage time (two months). In 90% of cases, brittle behavior is observed for all specimens printed in X and Y directions, while ductile behavior is performed for Z. Results confirmed that UCS, σ_t, and E of the 3DP specimens are highly dependent on the saturation binder rate (W) and the printing direction. In detail, UCS, σ_t, and E increase with the increase of the saturation binder rate, and the maximum properties are systematically measured for specimens printed in the Y direction, therefore the material behavior is considered to be anisotropic (Fig. 2 and Fig. 3).

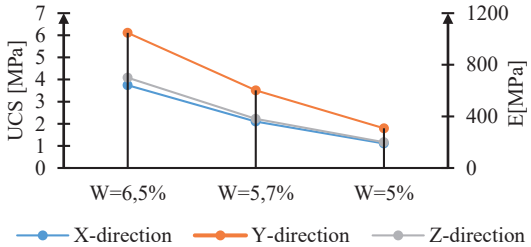

Fig. 2. UCS and Yong's Modulus (E) of 3DP cylindrical specimens function of the binder rate (W)

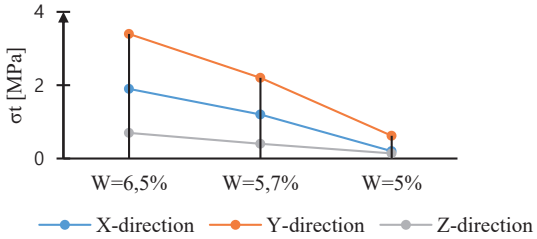

Fig. 3. Tensile strength (σ_t) of 3DP bars specimens function of the binder rate (W)

The scaling factors calculation between the prototype model and the scaled physical model are based on the Vaschy-Buckingham theorem (Buckingham, 1914; Jaber, 2020), (Table 1) where $P^* = P_p/P_m$ with P_p the value of the prototype parameters (real scale) and P_m the value of the model parameters (reduced scale). For those calculations, we measured an average bulk density of the 3DP material of 13kN/m^3 with a standard deviation equal to 0.5kN/m^3. This value is independent of the printing direction and binder saturation level. After applying the scale relationships, a binder saturation rate (W) equal to 5% is adopted to simulate a stiff to very stiff natural intact rock, with low to high UCS.

Table 1. The experimental range for artificial intact rock parameters and their corresponding values at prototype scale for three scale factors: 10, 25, and 50.

$\gamma_m = 13\text{kN/m}^3$, $20\text{kN/m}^3 < \gamma_p < 32\text{kN/m}^3 \Rightarrow \gamma^*_{moy} = \frac{\gamma_p}{\gamma_m} = 2$

Parameters	3D-printing (W=5%)	$L^* = 10$	$L^* = 25$	$L^* = 50$
E [GPa]	0.20-0.32	4.0-6.5	10.0-16.0	20.0-32.0
UCS [MPa]	1.1-1.8	20.0-35.0	55.0-90.0	110.0-180.0
σ_t [MPa]	0.1-0.6	2.0-12.0	5.0-30.0	10.0-60.0

3.1 Artificial 3DP joint

Before studying the feasibility of producing an artificial fractured rock mass, it is necessary to investigate the behavior of a single artificial joint. Many studies indicate that fractal surfaces with a self–affine replication have great potential to describe the surface roughness of a natural rock joint in granite, sandstone, or marble over several orders of magnitude (Candela et al., 2012; Y. Li et al., 2017; Odling, 1994; Zhang et al., 2019). Such surfaces satisfy a scale invariance and are statistically unchanged by transformation.

$$x \to \lambda\ x;\ y \to \lambda\ y;\ z(x,y) \to \lambda^H\ z(x,y) \qquad (1)$$

Where H is called the Hurst exponent related to the fractal dimensions D_f of the surface via $H=3-D_f$.

The power spectrum density (PSD) is used as a quantitative description to generate a self-affine rough surface (Nie et al., 2019; Persson, 2014). A set of ideal self-affine rough surfaces similar to a natural rock joint of dimension 150mm x 150mm are generated with the power spectrum density method. It includes six rough surfaces with the same roughness shapes but different values of the couple (H_i= 0.5-0.75-0.99; σ_j =0.75-1), where σ is the standard deviation of the surface elevation. By decreasing H and increasing σ the surface gets rougher (Fig. 4).

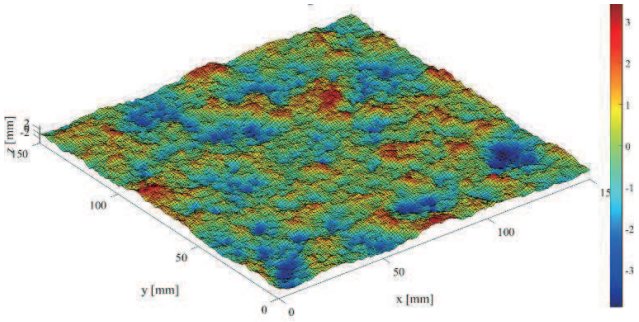

Fig. 4. Self-affine surface, with δx=δy=1mm, H=0.5; and σ=1mm

These surfaces were printed using a binder jetting process with a binder rate (W) equal to 5.7% in the Z-printing direction and then scanned using a 3D scanner with an accuracy of 50µm. The scanning results confirm that the printed surfaces are isotropic in the X-Y plane, and highlight the resolution limits of the binder jetting 3DP process; below the 8mm scale the 3DP process is not able to reproduce the required surface.

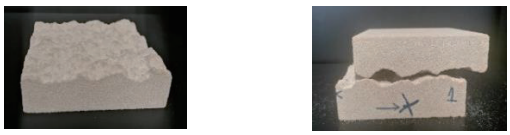

Fig. 5. Shear test specimens printed using the Binder Jetting process

The constructed joints underwent 20 direct shear tests, with constant normal stress equal to 0.4MPa, 0.8MPa, and 1.2MPa. Preliminary results revealed three behaviors depending on the applied normal stress (Fig. 6): (i) at low normal stress, about 10% of the UCS value, asperities with the larger wavelength cause dilation; (ii) at normal stress equal to 35% of the UCS value, tensile and/or slip cracks were observed in and under the longer wavelength asperities, which propagate within the intact matrix. These cracks are developed during the shearing process and lead to a joint closure in association with asperities crushing, and rock matrix plastic deformation; (iii) at normal intermediate stress equal to 25% of the UCS value, the two mechanisms were conjointly observed. It is noteworthy that the unevenness (i.e. small asperities) tends to be damaged in all cases. These mechanisms have already been observed in natural fractures (Bahaaddini et al., 2016; Huang et al., 2002).

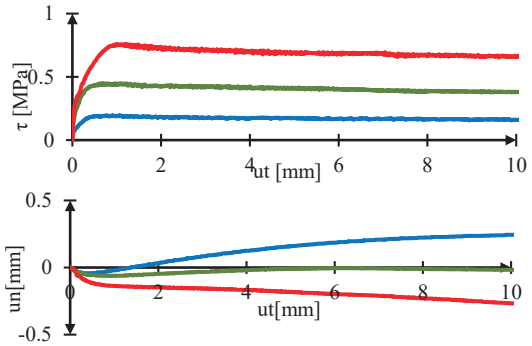

Fig. 6. Shear and dilation curves tests for (H=0.5 and σ=0.75) at different normal stresses: 1.2MPa (red), 0.8MPa (green), 0.4MPa (bleu), dilation behavior: when u_n increases with u_t, contraction behavior when u_n decreases with u_t

Data collected from 20 tests are used to estimate the cohesion and friction angles of the artificial joint hypothesizing that they follow a Coulomb behavior. The friction angle is equal to 31° with a standard deviation equal to 2° regardless of the fractal parameters, while the cohesion is closed to zero. This is compatible with the friction angle of a natural joint (Barton & Choubey, 1977; Hauquin, 2016).

3.3 Artificial random fractured rock mass

Fractured rock masses can be modeled with two different approaches (Hamdi et al., 2017): (i) a continuous medium, (ii) a discontinuous medium. This assumption depends on the block size (D_b) formed by the discontinuities intersections compared to the size of the structure (D_s), as well as the stress level within the rock mass (σ_{max}) compared to the rock mass compressive strength (UCS). In the present work, the rock mass is modeled with a discontinuous pattern and controlled a-priori by the formed block's behavior, which corresponds to ($1<D_s/D_b<10$ & $1<UCS/\sigma_{max}<100$). The blocks will therefore be connected by printed bridges.

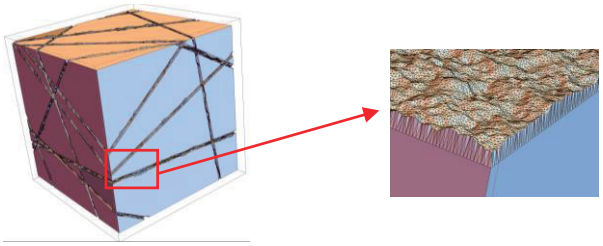

Fig. 7. a) 3D numerical random artificial fractured rock mass, b) numerical artificial rough rock joint

10 CONCLUSIONS

This study presents a new approach for producing a 3D reduced-scale physical model of an explicit stochastic fractured rock mass. 3DP based on sand and liquid binder mixture is used to reproduce the artificial rock mass with controllable geometrical and mechanical parameters. The mechanical parameters obtained from shear, compression, and tensile tests on our replica are translated to prototype scale by applying scaling relationships. The results show that the binder jetting 3DP with a 5% binder saturation rate successfully replicates the behavior of intact rock, and of joints and may be used to create a model of a rock mass with a scaling factor up to 50. Further on, a set of experimental tests will be performed on larger 3DP cylinder specimens with explicit fractures before realizing the physical model.

REFERENCES

Bahaaddini, M., Hagan, P. C., Mitra, R., & Khosravi, M. H. (2016). Experimental and numerical study of asperity degradation in the direct shear test. *Engineering Geology*, *204*, 41–52. https://doi.org/10.1016/j.enggeo.2016.01.018

Barton, N., & Choubey, V. (1977). The shear strength of rock joints in theory and practice. *Rock Mechanics Felsmechanik Mécanique Des Roches*, *10*(1–2), 1–54. https://doi.org/10.1007/BF01261801

Buckingham, E. (1914). On physically similar systems; Illustrations of the use of dimensional equations. *Physical Review*, *4*(4), 345–376. https://doi.org/10.1103/PhysRev.4.345

Candela, T., Renard, F., Klinger, Y., Mair, K., Schmittbuhl, J., & Brodsky, E. E. (2012). Roughness of fault surfaces over nine decades of length scales. *Journal of Geophysical Research: Solid Earth*, *117*(8), 1–30. https://doi.org/10.1029/2011JB009041

Fuenkajorn, K., & Phueakphum, D. (2010). Physical model simulation of shallow openings in jointed rock mass under static and cyclic loadings. *Engineering Geology*, *113*(1–4), 81–89. https://doi.org/10.1016/j.enggeo.2010.03.003

Hamdi, J., Scholtès, L., Souley, M., & Al Heib, M. (2017). Effect of discretization at laboratory and large scales during discrete element modelling of brittle failure. *International Journal of Rock Mechanics and Mining Sciences*, *100*(October), 48–61. https://doi.org/10.1016/j.ijrmms.2017.10.022

Hauquin, T. (2016). *La rupture brutale des piliers conditionne-t-elle les effondrements miniers ?* 247. http://files/79/Hauquin - 2016 - La rupture brutale des piliers conditionne-t-elle .pdf

Huang, T. H., Chang, C. S., & Chao, C. Y. (2002). Experimental and mathematical modeling for fracture of rock joint with regular asperities. *Engineering Fracture Mechanics*, *69*(17), 1977–1996. https://doi.org/10.1016/S0013-7944(02)00072-3

Jaber, J. (2020). *Application de la fabrication additive à la modélisation physique des joints et des massifs rocheux , par approches expérimentales et numériques. Thèse de Doctorat de l'Université de Lorraine, Nancy, France.*

Jacques-hulin, M. (2019). *Développement d'une méthode de conception de moules hybrides en fonderie. Thèse de Doctorat de l'univerité de Reims Champagne-Ardenne, France.*

Li, Y., Oh, J., Mitra, R., & Canbulat, I. (2017). A Fractal Model for the Shear Behaviour of Large-Scale Opened Rock Joints. *Rock Mechanics and Rock Engineering*, *50*(1), 67–79. https://doi.org/10.1007/s00603-016-1088-8

Li, Z., Liu, H., Dai, R., & Su, X. (2005). Application of numerical analysis principles and key technology for high fidelity simulation to 3-D physical model tests for underground caverns. *Tunnelling and Underground Space Technology*, *20*(4), 390–399. https://doi.org/10.1016/j.tust.2005.01.004

Nie, Z. hong, Wang, X., Huang, D. liang, & Zhao, L. heng. (2019). Fourier-shape-based reconstruction of rock joint profile with realistic unevenness and waviness features. *Journal of Central South University*, *26*(11), 3103–3113. https://doi.org/10.1007/s11771-019-4239-8

Nyembwe, K., Mashila, M., van Tonder, P. J. M., de Beer, D. J., & Gonya, E. (2016). Physical properties of sand parts produced using a voxeljet vx1000 three-dimensional printer. *South African Journal of Industrial Engineering*, *27*(3SpecialIssue), 136–142. https://doi.org/10.7166/27-3-1661

Odling, N. E. (1994). Natural fracture profiles, fractal dimension and joint roughness coefficients. *Rock Mechanics and Rock Engineering*, *27*(3), 135–153. https://doi.org/10.1007/BF01020307

Perras, M. A., & Vogler, D. (2019). Compressive and Tensile Behavior of 3D-Printed and Natural Sandstones. *Transport in Porous Media*, *129*(2), 559–581. https://doi.org/10.1007/s11242-018-1153-8

Persson, B. N. J. (2014). On the fractal dimension of rough surfaces. *Tribology Letters*, *54*(1), 99–106. https://doi.org/10.1007/s11249-014-0313-4

Son, M., & Park, J. (2014). Physical and numerical tests of the excavation walls in jointed rock masses. *Canadian Geotechnical Journal*, *51*(5), 554–569. https://doi.org/10.1139/cgj-2013-0081

Stone, K. J. L., & Taylor, R. N. (1965). *Modelling of Fractured Rock Masses*.

Tao, M., Hong, Z., Peng, K., Sun, P., Cao, M., & Du, K. (2019). Evaluation of excavation-damaged zone around underground tunnels by theoretical calculation and field test methods. *Energies*, *12*(9). https://doi.org/10.3390/en12091682

Thanh, T., & Hoang, N. (2013). *Etude du comportement d'un milieu rocheux fracturé : Application à la réalisation du tunnel de St Béat. Thèse de Doctorat de l'Ecole Des Ponts ParisTech, Paris, France.*

Xu, D., Huang, X., Jiang, Q., Li, S., Zheng, H., Qiu, S., Xu, H., Li, Y., Li, Z., & Ma, X. (2021). Estimation of the three-dimensional in situ stress field around a large deep underground cavern group near a valley. *Journal of Rock Mechanics and Geotechnical Engineering*, *13*(3), 529–544. https://doi.org/10.1016/j.jrmge.2020.11.007

Yingjie, L., Zhang, D., Fang, Q., Yu, Q., & Xia, L. (2014). A physical and numerical investigation of the failure mechanism of weak rocks surrounding tunnels. *Computers and Geotechnics*, *61*, 292–307. https://doi.org/10.1016/j.compgeo.2014.05.017

Zhang, X., Jiang, Q., Kulatilake, P. H. S. W., Xiong, F., Yao, C., & Tang, Z. (2019). Influence of asperity morphology on failure characteristics and shear strength properties of rock joints under direct shear tests. *International Journal of Geomechanics*, *19*(2), 1–13. https://doi.org/10.1061/(ASCE)GM.1943-5622.0001347